Cement and Concrete Research 39 (2009) 950–956

Contents lists available at ScienceDirect

Cement and Concrete Research

journal homepage: http://ees.elsevier.com/CEMCON/default.asp

Porosity and specific surface area of Roman cement pastes

Renata Tišlova [a], Antonina Kozłowska [b], Roman Kozłowski [b,*], David Hughes [c]

[a] Faculty of Restoration, University of Pardubice, Jiraskova 3, 57001 Litomysl, Czech Republic
[b] Institute of Catalysis and Surface Chemistry, Polish Academy of Sciences, Niezapominajek 8, 30-239 Kraków, Poland
[c] School of Engineering, Design and Technology, University of Bradford, Richmond Road, Bradford BD7 1DP, UK

ARTICLE INFO

Article history:
Received 29 November 2007
Accepted 18 June 2009

Keywords:
(B) Mercury porosimetry
(B) Pore size distribution
(B) Surface area
(D) Cement paste
(D) Roman cement

ABSTRACT

Mercury porosimetry, water vapour and nitrogen adsorption were used to follow the hydration of Roman cements — belite cements calcined at low temperature. Generally, unimodal distribution of pore sizes was observed, with the threshold pore width decreasing considerably with increasing curing time. An open porous structure with the threshold pore diameter between 0.2 and 0.8 μm and the specific surface area not exceeding 20 m^2/g was produced at early ages when quick growth of the C–A–H phases is observed. The surface area reached up to 120 m^2/g and the threshold pore width shifted to around 0.02 μm when the subsequent formation of C–S–H gel filled the larger pores. Both mercury porosimetry and water vapour adsorption were found to be capable of following the progress of hydration of the Roman cements with high reliability at least for a comparative evaluation of historic Roman cement mortars and repair materials used in restoration projects.

1. Introduction

This is the second of a series of papers on the composition and hydraulic nature of Roman cements, highly hydraulic binders widely applied during the nineteenth and early twentieth centuries in construction, especially for the economic and easy manufacture of stuccoes for the exterior of buildings. Roman cements were produced by calcining naturally occurring limestones rich in clay minerals below the sintering point and then grinding the burnt material to a fine powder. Their characteristic mineralogy, which is the product of several solid-state reactions taking place during the burning process, is presented in detail in the first paper of the series [1]. One notable feature is the transformation of $\alpha'C_2S$ to βC_2S as the stable form of belite as the calcination temperature of cements is raised. The same paper describes strength development during the hydration of Roman cement pastes which proceeds according to a two-step mechanism:

Step 1 Roman cement pastes harden within a few minutes after the initial set. Six-hour strength values of up to 4 MPa are obtained.
Step 2 After a varying dormant period, depending on the type of Roman cement and calcination conditions, further strength development leads to high final strength values — after 1 year compressive strengths exceeding 20 MPa were measured.

The in-situ X-ray diffraction of the Roman cement pastes [2] revealed a correlation between the early strength development and the formation of crystalline calcium aluminum oxide carbonate (or carbonate hydroxide) hydrates (C–A–H). Optical and SEM microscopy of historic Roman cement mortars has shown that the formation of a dense microstructure accounting for their final strength is due to the hydration of belite yielding calcium silicate hydrates — the C–S–H gel [3].

Mercury porosimetry is used in this paper to study the growth of the C–S–H gel into the pore space of hardened cement pastes. Further, adsorption of water vapour and nitrogen is used to determine the amounts of the hydrated products formed as a function of the curing time.

The paper focuses on verifying the potential of these techniques to follow the progress of the hydration of Roman cement pastes and mortars with high reliability and precision at least for a comparative evaluation of similar materials. The characteristics of the pore structure of the hydrated cements is an important indicator of the properties and behaviour of historic mortars or the repair materials which are expected to vary with the exposure of the specimen surface to different external environments. The lack of moisture may result in restricted hydration and affect the porosity and strength of the mortars. Quantifying such an influence would be of great importance for the practical application of Roman cements in the conservation of historic mortars, as ideal wet curing of mortars is rarely possible in the course of practical work on the facades of buildings.

2. Materials and methods

2.1. Materials

Three Roman cements were studied. All were burnt at the laboratory of the School of Engineering, Design and Technology, University of Bradford, UK, as described in [1]. The cements were burnt either from the Lilienfeld marl, Austria, or from the Folwark marl, Poland. The burning conditions and oxide compositions are given in Table 1. The combination

* Corresponding author. Tel.: +48 12 6395119; fax: +48 12 4251923.
E-mail address: nckozlow@cyf-kr.edu.pl (R. Kozłowski).

0008-8846/$ – see front matter © 2009 Elsevier Ltd. All rights reserved.
doi:10.1016/j.cemconres.2009.06.020

Table 1
Chemical composition of Roman cements investigated, weight %.

Cements	SiO_2	Al_2O_3	Fe_2O_3	CaO	MgO	SO_3	Na_2O	K_2O	TiO_2	Loss on ignition	Free lime
Folwark 820 °C 400 min	27.9	6.9	2.5	48.2	1.6	0.6	0.3	1.5	0.4	10.0	6.4
Folwark 960 °C 300 min	29.9	7.3	2.8	51.3	1.9	0.8	0.3	1.5	0.4	3.7	6.4
Lilienfeld 920 °C 300 min	29.1	9.2	3.6	46.8	1.5	0.0	0.7	2.1	0.4	6.5	0.2

of temperature and time was used to classify each cement (e.g. 920/300). The pastes were produced at the water–cement ratio of 0.65. The value of water–cement ratio was practically determined as being that which yielded a paste of sufficient fluidity to allow the casting of the most rapidly setting pastes into the moulds before the onset of the setting process. It has also been the value commonly used by participating restorers preparing mortars for the production of cast elements.

2.2. Methods

Wet chemical analyses to determine oxide composition of cements studied followed the procedures of the European Standard EN 196-2: 2005. X-ray diffraction analysis used to determine their mineralogy as well as the measurements of strength are described in [1].

For porosity structure measurements, prismatic specimens of $20\times2\times2$ cm were cast in steel moulds. The samples were demoulded immediately after setting and cured over distilled water i.e. near 100% relative humidity until tested. Organic solvent exchange was used to dry specimens after the specified hydration time, as our preliminary tests showed that this drying method best preserved the paste microstructure in the region of the smallest pores as analysed with mercury intrusion porosimetry. The specimens were removed from the climatic chamber and immediately soaked in acetone for 24 h. They were then placed in a rotary vacuum flask at 20 °C for 4 h to remove acetone and to be dried. The pore structure of the paste samples was determined using a PoreMaster 60 mercury intrusion porosimeter from Quantachrome, which generates pressure to 60,000 psia or 400 MPa for pore size analysis from 440 to 0.0035 μm pore diameter.

The same paste samples were used for water vapour adsorption measurements which were conducted gravimetrically for the relative pressure range 0–0.98 with the use of a Sartorius vacuum microbalance at 24 ± 0.2 °C. Typically about 0.1 g of a sample was used for each experiment. The sample was evacuated for 3.5 h at 10^{-3}Torr at the temperature of the measurement to remove physically adsorbed water and maintain the microstructure obtained during the organic solvent exchange procedure. Then portions of water vapour were added until the required relative pressure was attained and the corresponding mass increase of the sample was recorded. After the saturation water vapour pressure had been reached, the desorption branch was measured. On average, 15 points were measured on the adsorption branch of the isotherm and 10 points on the desorption branch, and approximately 1 week was necessary for the complete measurement. Water vapour accessible surface area was calculated using the BET equation [4] over a relative pressure range from 0.05–0.3. In the determination of the BET surface area a cross-sectional area of 0.114 nm^2 for the water molecule was used. The *t*-method, proposed first by Lippens and deBoer [5], was also used to determine the water vapour accessible surface area and the *t*-curves employed are specified in section 3.4 below.

Nitrogen adsorption was performed using an Autosorb-1 from Quantachrome. Surface area was calculated using the BET equation over a relative pressure range from 0.05 to 0.3.

Table 2
Mineralogical composition of Roman cements investigated, weight %.

	Folwark 820 °C/400 min	Folwark 960 °C/300 min	Lilienfeld 920 °C/300 min
Quartz	5	4	4
Calcite	16	0	6
Portlandite	10	6	0
α′-belite	36	9	30
β-belite	4	50	20
Gehlenite	0	15	4
Total crystalline phases	71	84	64
Amorphous components	29	16	36

3. Results and discussion

3.1. Chemistry and mineralogy of the Roman cements studied

The oxide composition of the cements studied is given in Table 1. The mineralogical composition of cements is shown in Table 2. Ratio of crystalline to amorphous or poorly crystalline phases was quantified by adding an internal standard in the X-ray diffraction analysis; the results are expressed as relative amounts of all identified crystalline phases and the amorphous component in percents. They show a considerable progress of the reactions taking place during calcination of the marls; principally, the decomposition of calcite to lime and its reaction with quartz and clay decomposition products to give belite and, at higher temperatures, gehlenite. The Folwark Roman cement 820/400 has a mineralogical composition characteristic of comparatively low temperatures of burning. It retains a considerable amount of undecomposed calcite and free unreacted lime, which has transformed to calcium hydroxide — portlandite — by reaction with moisture contained in the air. A characteristic feature is a high proportion of α′-belite dominating at low calcinations, very little β-belite and no gehlenite. It contains also a substantial amount of amorphous or poorly crystalline phases. As no crystalline aluminate phases were observed despite selective dissolution of silicates and free lime in salicylic acid and methanol [2], the source of aluminates is believed to be within the amorphous phase. When, however, the Folwark marl undergoes a more intense calcination (here 960 °C for 300 min), a considerable change in its mineralogical composition is observed. The calcite decomposes completely and contents of both β-belite and gehlenite increase at the expense of the amorphous phase and α′-belite. The Lilienfeld cement can be placed somewhat between the two Folwark cements as indicated by a moderate decrease in the calcite content and increase in both β-belite and gehlenite.

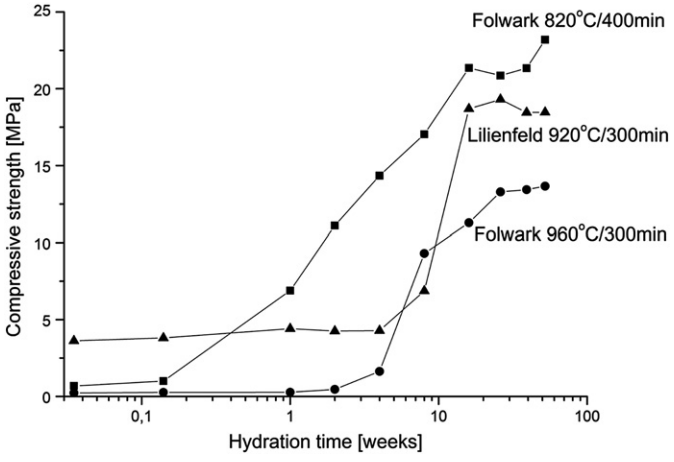

Fig. 1. Strength development profiles of the pastes of the Roman cements studied.

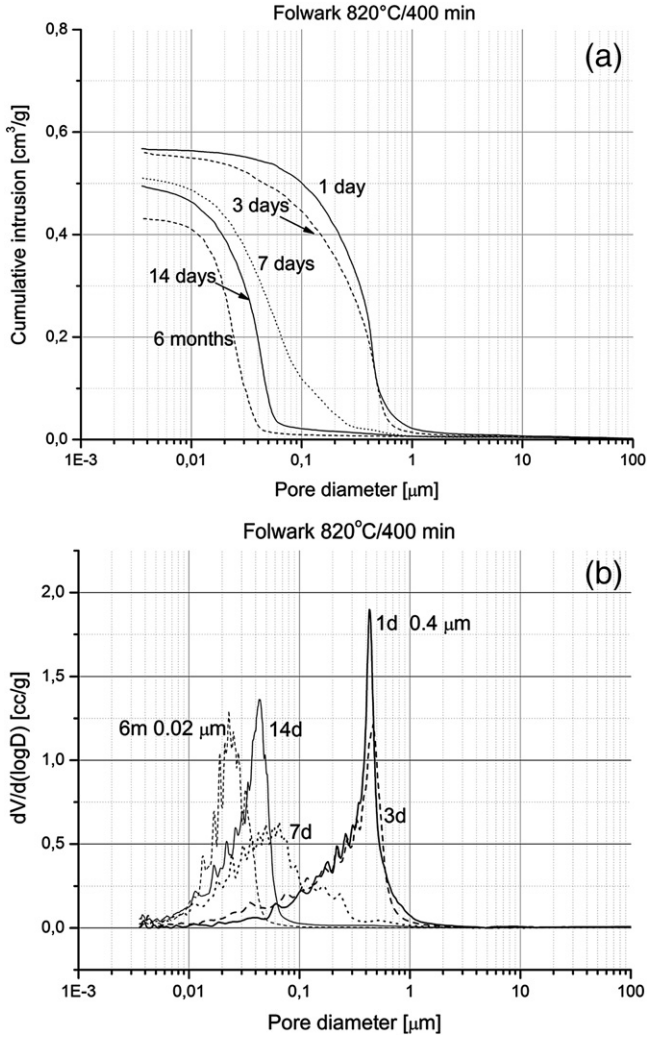

Fig. 2. Cumulative (a) and differential (b) volume of intruded mercury vs pore diameter for the paste made of the Folwark 820/300 Roman cement cured at various ages.

3.2. Strength development

Given the historical experience and the results reported in [1] three zones of calcination of Roman cements can be classified: optimal which coincides with the highest four-week strength and the most rapid setting, sub-optimal at lower temperatures and super-optimal at higher temperatures. Folwark 820/400 and Lilienfeld 920/300 are classified as optimal cements whilst Folwark 960/300 is a super-optimal cement. The strength development profiles for all three cements are shown in Fig. 1; the coefficient of variation in measured strengths was typically in the range 2–8%. Generally, the profiles consist of three stages. Within the first 6 h all pastes attain early strength which, however, is approximately five times higher for the Lilienfeld paste than for the Folwark. This first stage of hardening is followed by a dormant period which is negligible for the Folwark 820/300 (less than 24 h), lasts in the case of the Lilienfeld cement for more than 5 weeks and for the intensely calcined Folwark 960/300 for about 3 weeks. The dormant periods are followed by the accelerated strength gain to the same level of approximately 20 MPa for the optimal cements and 14 MPa for the super-optimal cement.

The much higher early strength of the Lilienfeld pastes when compared to the Folwark pastes is the result of a more abundant formation of the C–A–H phases [2]. The long-term strength correlates with the formation of calcium silicate hydrates — the C–S–H gel. Its formation and growth into the pore space of hardened cement pastes is studied in detail in the present paper with the use of mercury porosimetry and water vapour adsorption.

3.3. Pore structure of the pastes

Figs. 2–4 compare the cumulative and differential mercury intrusion curves i.e. cumulative and incremental pore volume intruded as a function of pore diameter for the pastes of the three Roman cements studied at several ages between 15 min and 1 year. The differential mercury intrusion curves of the Roman cements hydrated at early ages exhibit a single, sharply defined peak at a pore diameter from 0.2 to 0.8 μm. The presence of the peak indicates a one-step intrusion of mercury into a capillary network connected to the specimen surface. It corresponds to the minimum throat dimension of this network — the 'critical' or 'threshold' diameter according to [6]. Cook and Hover determined systematically the threshold pore widths for Portland cement pastes as a function of *w*/*c* ratio and curing time [7]. They varied between approximately 2 and 0.02 μm and, as expected, smaller values were obtained with increased curing time and decreased *w*/*c* ratio. The values for 1 day pastes clustered between 2 and 0.4 μm for *w*/*c* ratios between 0.7 and 0.4; only the 0.3 *w*/*c* paste did not exhibit the initial mercury intrusion peak, corresponding to a large threshold pore width, at any curing period tested.

The pore structure of the young Roman cement pastes correlates with the strength development profiles in the pastes. The initial single

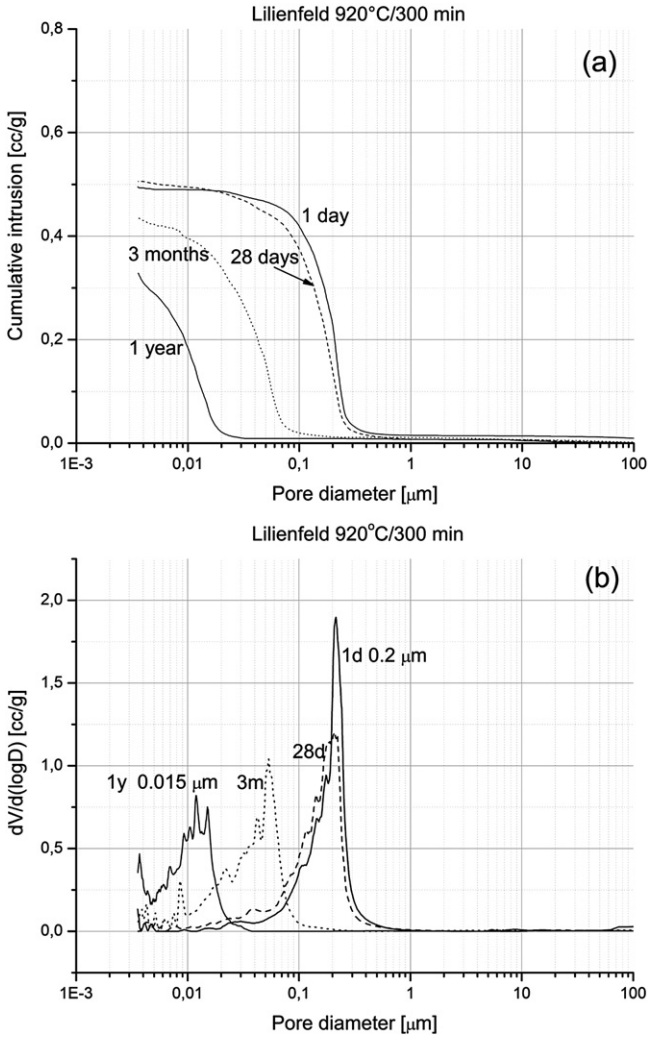

Fig. 3. Cumulative (a) and differential (b) volume of intruded mercury vs pore diameter for the paste made of the Lilienfeld 920/400 Roman cement cured at various ages.

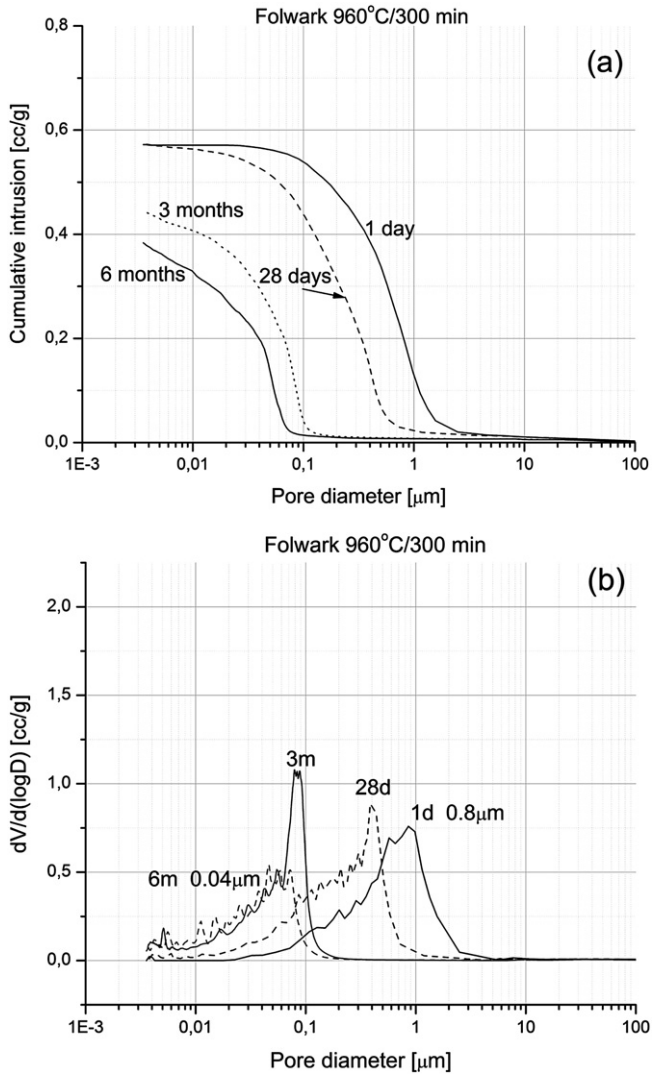

Fig. 4. Cumulative (a) and differential (b) volume of intruded mercury vs pore diameter for the paste made of the Folwark 960/300 Roman cement cured at various ages.

peak appears in the pastes cured for the least amount of time and remains unchanged during the dormant period of the paste which can extend up to several weeks. Only then does the peak shift to smaller pore sizes, which is assumed to be the result of filling of larger pores by the formation of C–S–H gel. The same correlations are observed for the cumulative intruded pore volume curves.

Though all pastes at early curing times exhibit a unimodal distribution of the throat pore dimensions, the actual threshold pore width varies between different cements. It is the smallest for the Lilienfeld cement, yielding high early strength, and the largest for the intensely calcined Folwark cement 960/300, yielding early strength five times lower than Lilienfeld. Pastes of a rapidly-hydrating calcium sulfoaluminate cement, capable of the very fast development of hydration products, ettringite and aluminum hydroxide, showed a similar threshold diameter at early ages [8]. The correlation between the total intruded pore volumes and the strength development profiles is less pronounced though the minimum values of the total porosity are observed again for the Lilienfeld cement. It should be stressed at this point that the paste samples used for the strength measurements were cured under water [1] whilst those used in the mercury intrusion work were wet-air cured as described in section 2.2. Though the curing conditions were not identical, the broad trends of hydration and strength development are similar such that general correlations are valid.

When the curing time exceeds the dormant period of any given cement, the initial peak shifts to smaller pore sizes between 0.05 and 0.01 μm, and the total intruded pore volume decreases. The parallel increase in strength indicates that the process involves filling the larger pores by the formation of C–S–H gel. The pore sizes agree well with the data given in the literature for matured cement pastes in which hydration products grow into the pore space. In particular, Cook and Hover have shown that the threshold pore widths for Portland cement pastes cluster between 0.2 and 0.02 μm at curing times of 56 days for *w*/*c* ratio decreasing from 0.7 to 0.3 [7]. Fig. 5 shows the mercury intrusion curves for the pastes of the ordinary Portland cement (OPC) studied at ages between 1 day and 6 months. The threshold pore width of matured, six-month-old OPC paste is 0.01 μm, similar to the same data for matured pastes of optimal Roman cements (Folwark 820/400 at 6 months and Lilienfeld 920/300 at 1 year). However, the pore structure development of the OPC paste is somewhat different. The total intruded pore volumes are lower than those of any of Roman cement pastes. The initial threshold pore width is 1 μm. However, a bimodal distribution of pore sizes is achieved quickly, pointing to the quick formation of the regions of lower porosity due to the C–S–H growth. In the Roman cements the C–S–H gel is generated more slowly so it only gradually refines the pore structure, which is reflected in a continuous shift of the pore network to lower threshold pore widths, rather than the appearance of a bimodal distribution within the pore structure.

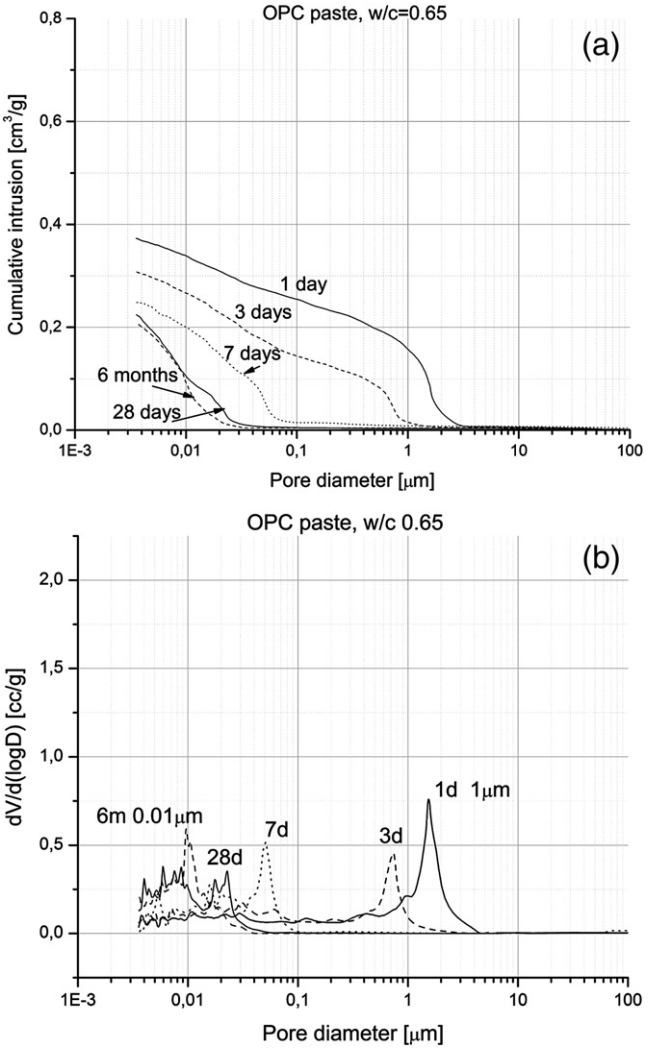

Fig. 5. Cumulative (a) and differential (b) volume of intruded mercury vs pore diameter for the paste made of the ordinary Portland cement cured at various ages.

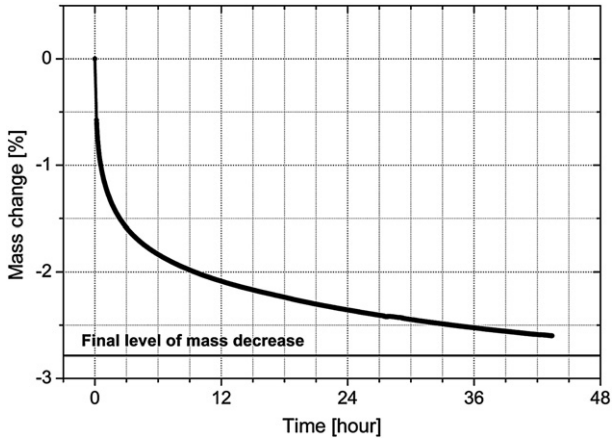

Fig. 6. Mass decrease vs period of outgassing for a 28-day-old paste of Lilienfeld 920/300.

3.4. Adsorption–desorption isotherms and specific surface areas accessible to H_2O and N_2

Adsorption of nitrogen and water vapour has been widely used for determining the specific surface area of hydrated cements. Factors that may affect the determination have been recently reviewed in detail by Odler [9] and further discussed in the subsequent two papers [10,11].

The first problem, which must be clearly addressed in any specific surface area determination procedure, is sample preparation. The adsorption of gases must start at a clean, well-defined, reproducible solid surface. Therefore each sample must be outgassed to remove air from the paste structure and to eliminate most of the species physisorbed during storage of the sample, including adsorbed water. A problem exists, however, in the limited possibility to separate the water physisorbed on the surface of the existing pores without simultaneously removing some strongly bound water present in aluminate and silicate hydrates or as interlayer water within their structure. By way of example, Fig. 6 shows a mass decrease, as a function of time of outgassing at 24 °C, for the paste of the Lilienfeld cement 920/300 cured for 28 days. As can be seen, the plot follows an exponential type function and the final mass decrease for the sample stored in the laboratory environment is estimated at 2.8% from the experimental data. The release of water is continuous but is especially intense within the first 3 h of the outgassing, during which time the weakly bound water is removed.

The subsequent measurements of the adsorption isotherms for samples outgassed for two periods of time, 3.5 and 42 h, shown in Fig. 7,

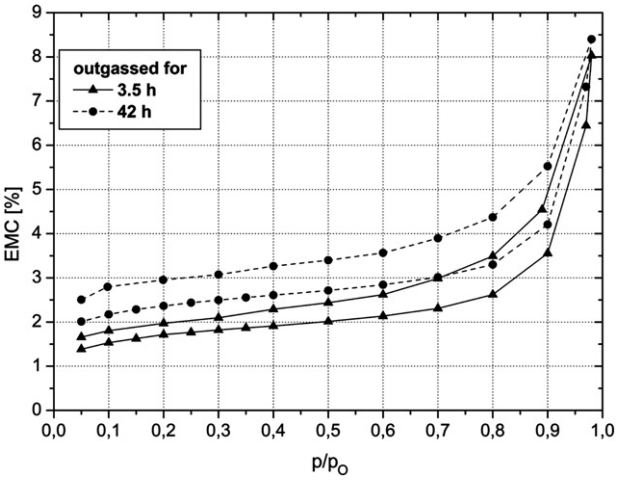

Fig. 7. Adsorption–desorption isotherms of water vapour on the paste of Lilienfeld 920/400 Roman cement cured for 28 days, outgassed for 3.5 and 42 h. EMC — equilibrium moisture content, p/p_o — relative pressure of water vapour.

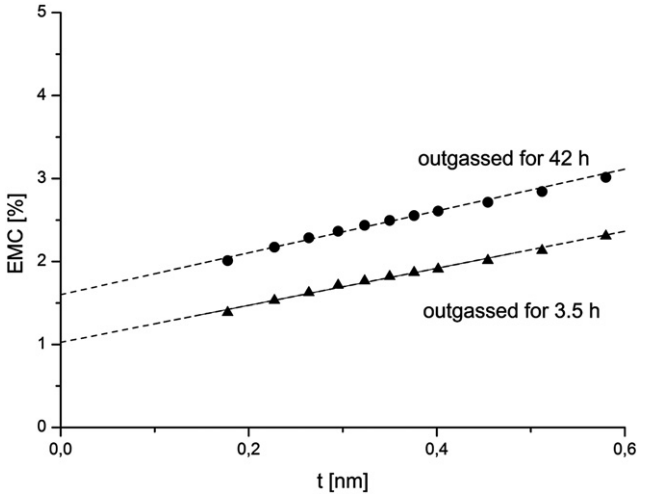

Fig. 8. EMC–t plot of the adsorption data shown in Fig. 7. EMC — equilibrium moisture content, t — statistical thickness of the adsorbed water layer.

reveal that strongly bound water and physically adsorbed water can be separated by the following processing of the adsorption data. The adsorption consists of two components. There is an irreversible initial uptake of the first portions of water vapour dosed to the system until the re-hydration of the structure due to strong water–surface interactions is reached. Then a physical adsorption of water vapour occurs described by the sigmoid shape of the type II isotherm in the IUPAC 1985 classification [12]. It indicates a progressively thickening adsorbed water layer as the vapour pressure is increased up to the saturation pressure, at which the adsorbed layer becomes a bulk liquid. It can be read from the figure that the physical adsorption part is the same for varying outgassing periods but it is displaced vertically along the y-axis as levels of the initial re-hydration of the surface increase with increasing depletion of the surface of water by the outgassing.

The adsorption isotherms are easier to interpret if the p/p_o values on the ordinate axis are replaced by those of t, the statistical thickness of the water layer adsorbed on the suitable nonporous material of known specific surface area:

$$t(p/p_o) = \frac{V_{ads}}{S_{BET}} \quad (1)$$

The first universal $t(p/p_o)$ curves for water vapour were published by Hagynassy et al. [13]. Later, t-curves were proposed to be a function of

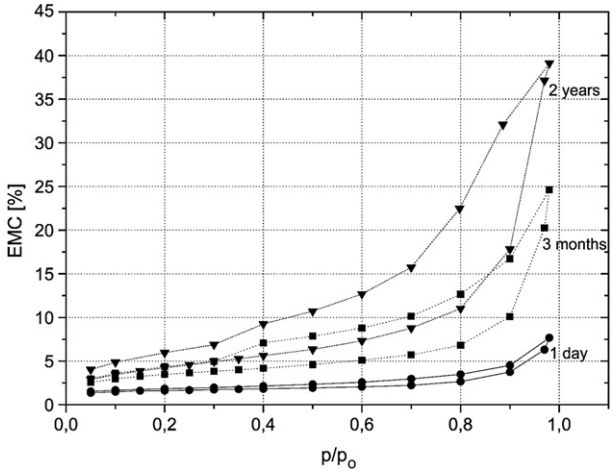

Fig. 9. Adsorption–desorption isotherms of water vapour on the paste of Lilienfeld 920/400 Roman cement cured at various ages. Definitions of EMC and p/p_o as in Fig. 7.

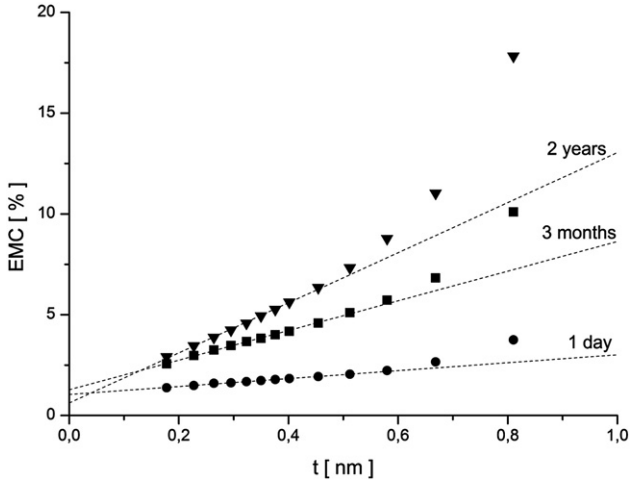

Fig. 10. EMC–t plot of the adsorption data shown in Fig. 9. Definition of EMC and t as in Fig. 8.

the chemical nature of the adsorbent and therefore many t-curves were measured to serve as standards to materials of similar chemistry. Badmann et al. used non porous di- and tri-calcium silicates to determine statistical thickness of the adsorbed water layer between 0.01 and 0.95 p/p_o and proved their suitability in interpreting the water sorption isotherms of hardened cement pastes [14]. Their t curve was expressed by a simple two-parameter equation:

$$t(p/p_o) = 3.85 - 1.89\ln(-\ln(p/p_o)) \quad (2)$$

which will be used to interpret water isotherms of the pastes studied in this paper.

The same EMC–p/p_o adsorption isotherms as in Fig. 7 are shown in Fig. 8 as EMC–t plots where EMC stands for the equilibrium moisture content expressed in per cent by mass. Since the volume adsorbed is a product of surface area and water layer thickness, a straight line graph is obtained as long as the water layer can grow freely on the entire surface of the sample. The straight line should go through the origin and its slope represents a water vapour accessible surface area. The slope is identical for the two plots and hence the surface area values are the same irrespectively of the outgassing time. However, upward displacements of the EMC–t plots are observed due to the initial uptake of water vapour during the re-hydration of the specimens.

The important conclusion of the above measurements is that the amount of water adsorbed physically does not depend on the outgassing schedule. Three hours under a vacuum of a residual pressure of less than 10^{-3} mbar were selected somewhat arbitrarily for further measurements.

Isotherms of adsorption–desorption of water vapour are shown in Fig. 9 for several pastes of the Lilienfeld cement 920/300, cured for times of up to 2 years. The isotherm for 28-day paste was identical to that of the 1-day paste and was not included in the figure. There is a characteristic evolution of the isotherms with the time of hydration. The adsorption–desorption isotherms of the young pastes, containing mainly the C–A–H phases, show relatively small water vapour uptake without a significant hysteresis loop, which indicates an open porous structure with no narrow entrances or 'ink bottle pores.' No evolution of the pore structure formed at the outset of hydration was observed until the end of the dormant period is reached and the C–S–H gel starts to grow. The matured pastes which contain growing amounts of the C–S–H gel show increasing water vapour uptake and a characteristic hysteresis loop reducing to negligible proportions at about $p/p_o = 0.35$ which points to a dense microstructure with 'ink bottle pores' [15].

The same EMC–p/p_o adsorption isotherms as in Fig. 9 are shown in Fig. 10 as the EMC–t plots. The straight line graphs are obtained as long as the water layer grows freely on the entire surface of the sample. Their slopes represent the water vapour accessible surface areas that include the walls of pores provided that the distance between opposing walls is large compared with molecular dimensions. However, when the water layer formation is accompanied by excess capillary condensation, an upward deviation in EMC–t plots is observed, due the presence of an extra amount of water when compared to the standard.

Table 3 shows the specific surface area of the pastes investigated as determined by several methods: $S_{t\ H2O}$ calculated from the EMC–t plots for water vapour adsorption as described above, BET_{H2O} and BET_{N2} calculated using the water and nitrogen adsorption data in the low pressure range and a least-square fit for the linearised two-parameter BET equation, and S_{Hg} cumulative pore surface area of pores accessible to mercury at pressures equivalent to a minimum pore size of 3.5 nm calculated under the assumption of a cylindrical pore geometry. The adsorption data used to calculate the BET_{H20} values were those of the 'pure' physical adsorption of water vapour which were obtained by subtracting from the raw measurements the irreversible initial uptake of the water vapour due to the re-hydration of the structure, determined from the EMC–t plots as shown in Fig. 8.

Several conclusions can be drawn from the results shown in Table 3. First, an excellent agreement between BET_{H20} and $S_{t\ H20}$ clearly points to the reliability of both the calculation of the BET areas and the t curve of Badman et al. [14] relating the statistical thickness of the adsorbed water layer to the relative pressure, used for the interpretation of the sorption isotherms. As a result, the obtained

Table 3
Specific surface area of the Roman cement pastes cured at various times as determined by different experimental methods.

Cement	Hydration time	$S_{t\ H2O}$ [m^2/g]	BET_{H20} [m^2/g]	BET_{N2} [m^2/g]	S_{Hg} [m^2/g]
Folwark 820 °C 400 min	15 min	10.0	10.0	10.7	–
	7 days	37.9	38.0	51.3	63.3
	28 days	61.5	58.8	41.7	82.0
	3 months	67.5	65.5	54.2	73.0
	6 months	70.9	69.3	37.9	92.8
	2 years	123.8	111.4	54.7	98.7
Folwark 960 °C 300 min	15 min	13.7	13.7	7.0	–
	28 days	27.8	26.8	22.0	25.4
	3 months	85.3	84.7	38.6	63.5
	6 months	93.3	93.4	36.3	80.0
	2 years	97.7	98.7	38.7	–
Lilienfeld 920 °C 300 min	15 min	13.7	13.7	11.7	–
	1 day	19.7	19.9	11.5	18.7
	28 days	21.7	23.2	16.4	27.5
	3 months	73.6	73.6	26.5	72.9
	6 months	109.1	105.0	46.1	102.6
	2 years	124.3	122.3	51.7	115.5

values of the water vapour accessible surface areas can be taken as reliable and useful indicators of the growth of the hydration products at least for a comparative evaluation of several cements which is the focus of the present investigations. The water vapour accessible surface areas are believed to represent the total surface of the pastes at all stages of the hydration [9]. In the case of Roman cements, the initial stage of hydration, involving the formation of the crystalline C–A–H phases, leads to a surface area not exceeding approximately 20 m^2/g. Formation of the C–S–H gel brings about an increase of the surface area up to 120 m^2/g, the value reflecting the amount of the C–S–H gel formed. The measurements of the amount of water vapour adsorbed open a possibility of following the progress of the hydration in the Roman cement pastes and mortars, and in particular of determining the amount of C–S–H present as suggested earlier by Olson and Jennings [16]. The profile of the development of the surface area correlates well with the strength development profiles of the individual pastes on the one hand and the pore structure evolution on the other. However, it should be noted that a single relationship between strength and surface area, applicable to all 3 of the pastes, has not been identified in this work.

The BET specific surface areas determined with nitrogen as the adsorbate are close to those found by water vapour adsorption only during the early stage of hydration corresponding to the formation of the open structure of the C–A–H phases. When the growth of the C–S–H gel is initiated the BET_{N2} values become consistently lower than those found by water vapour adsorption. The process has been thoroughly interpreted by many authors and reviewed recently by Odler [9] as being due to the formation of denser and more interwoven pore space which is totally or partially impermeable to N_2 molecules.

A generally close agreement is observed between the specific surface areas determined by mercury porosimetry with those found by water vapour adsorption, irrespectively of the degree of the paste hydration. As the method allows determination only of the surface of those pores into which mercury has penetrated, it reveals that multilayer physical adsorption of water is located in pores with diameter above about 3.5 nm.

4. Conclusions

The pastes of Roman cements showed a characteristic development of the pore structure. Generally, unimodal distribution of pore sizes was observed, as indicated by the occurrence of one, usually well-defined peak in the plot of the derivative volume of the mercury intruded. However, the 'threshold' pore width related to the highest rate of mercury intrusion per change in pressure decreases considerably as the hydration time increases.

At early ages, relatively open porosity structure is produced by the quick growth of the C–A–H phases in the pastes with the threshold pore diameter between 0.2 and 0.8 μm. The smaller threshold pore diameters and total intruded pore volumes, i.e. denser microstructures, are produced by cements capable of formation of larger amounts of the C–A–H phases, whereas the threshold pore diameters increase for cements with less amounts of the aluminates active in the hydration.

The initial open structure remains unchanged during the dormant period of pastes which can extend up to several weeks. Only then does the threshold pore width shift to smaller values concentrated around 0.02 μm, which is the result of filling larger pores by the formation of the C–S–H gel.

The evolution of the porosity structure correlates well with the development of the water vapour accessible surface area which is believed to represent the total surface of the pastes at all stages of the hydration. In the case of the Roman cements, surface area of the early structure produced by the quick growth of the C–A–H phases does not exceed approximately 20 m^2/g. Formation of the C–S–H gel brings about an increase of the surface area up to 120 m^2/g.

The obtained results indicate that both mercury porosimetry and water vapour adsorption open a possibility of following the progress of the hydration in the Roman cement pastes and mortars with high reliability and precision at least for a comparative evaluation of the similar materials. These two experimental approaches have been used to characterize a broader range of Roman cement mortars, including both the historic samples collected from the facades of the historic buildings and the repair mortars used in the restoration works. The water vapour adsorption has proved a particularly promising measurement technique as it required minute specimens which could be easily withdrawn from historic objects especially from thin finishing layers and coatings based on the Roman cements.

Acknowledgments

A part of this research was carried out within the ROCEM project (contract EVK4-CT-2002-00084), supported financially by the European Commission 5th Framework Programme, Thematic Priority: Environment and Sustainable Development, Key Action 4: City of Tomorrow and Cultural Heritage. Further, this work was supported by a grant from the Polish Ministry of Science and Higher Education within the Sectorial Operational Programme 'Improvement of the Competitiveness of Enterprises.'

References

[1] D.C. Hughes, D. Jaglin, R. Kozłowski, D. Mucha, Roman cements — belite cements calcined at low temperature, Cem. Concr. Res. 39 (2009) 77–89.
[2] R. Vyskocilova, W. Schwarz, D. Mucha, D. Hughes, R. Kozlowski, J. Weber, Hydration processes in pastes of Roman and American natural cements, J. ASTM Int. 4 (2) (2007) Paper ID JAI100669, available online at www.astm.org.
[3] J. Weber, N. Mayr, K. Bayer, D.C. Hughes, R. Kozlowski, M. Stillhammerova, D. Ullrich, R. Vyskocilova, Roman cement mortars in Europe's architectural heritage of the 19th century, J. ASTM Int. 4 (8) (2007) Paper ID JAI100667, available online at www.astm.org.
[4] S. Brunauer, P.H. Emmet, E. Teller, Adsorption of gases in multimolecular layers, J. Am. Chem. Soc. 60 (1938) 309–319.
[5] R.C. Lippens, J.H. deBoer, Studies on pore systems in catalysts V. The *t* method, J. Catal 4 (1965) 319–323.
[6] S. Diamond, Mercury porosimetry. An inappropriate method for the measurement of pore size distributions in cement-based materials, Cem. Concr. Res. 30 (2000) 1517–1525.
[7] R.A. Cook, K.C. Hover, Mercury porosimetry of hardened cement pastes, Cem. Concr. Res. 29 (1999) 933–943.
[8] G. Bernardo, A. Telesca, G.L. Valenti, A porosimetric study of calcium sulfoaluminate cement pastes cured at early ages, Cem. Concr. Res. 36 (2006) 1042–1047.
[9] I. Odler, The BET-specific surface area of hydrated Portland cement and related materials, Cem. Concr. Res. 33 (2003) 2049–2056.
[10] H.M. Jennings, J.J. Thomas, A discussion of the paper "BET-specific surface area of hydrated Portland cement and related materials" by Ivan Odler, Cem. Concr. Res. 34 (2004) 1959–1960.
[11] I. Odler, Reply to the discussion by H.M. Jennings, J.J. Thomas of the paper "BET-specific surface area of hydrated Portland cement and related materials", Cem. Concr. Res. 34 (2004) 1961.
[12] K.S.W. Sing, D.H. Everett, R.A.W. Haul, L. Moscou, R.A. Pierotti, J. Rouquerol, T. Siemieniewska, Reporting physisorption data for gas solid systems with special reference to the determination of surface area and porosity, Pure Appl. Chem. 57 (1985) 603–619.
[13] J. Hagymassy, S. Brunauer, R.S. Mikhail, Pore structure analysis by water vapor adsorption, I. *t*-curves for water vapor, J. Colloid Interface Sci. 29 (1969) 485–491.
[14] R. Badmann, N. Stockhausen, M.J. Setzer, The statistical thickness and the chemical potential of adsorbed water films, J. Colloid Interface Sci. 82 (1981) 534–543.
[15] J. Hagymassy Jr., I. Odler, M. Yudenfreund, J. Skalny, S. Brunauer, Pore structure analysis by water vapor adsorption, III. Analysis of hydrated calcium silicates and Portland cements, J. Colloid Interface Sci. 38 (1972) 20–34.
[16] R.A. Olson, H.M. Jennings, Estimation of C–S–H content in a blended cement paste using water adsorption, Cem. Concr. Res. 31 (2001) 351–356.